HHS Public Access

Author manuscript

Proteins. Author manuscript; available in PMC 2016 May 01.

Published in final edited form as:

Proteins. 2015 May ; 83(5): 989–996. doi:10.1002/prot.24781.

Opposing Orientations of the Anti-Psychotic Drug Trifluoperazine Selected by Alternate Conformations of M144 in Calmodulin

Michael D. Feldkamp[1], **Lokesh Gakhar**[1,2], **Nisha Pandey**[1], and **Madeline A. Shea**[1,*]

[1]Department of Biochemistry, Roy J. and Lucille A. Carver College of Medicine, University of Iowa, Iowa City, Iowa 52242-1109, USA

[2]Protein Crystallography Facility, Roy J. and Lucille A. Carver College of Medicine, University of Iowa, Iowa City, Iowa 52242-1109, USA

Abstract

The anti-psychotic drug trifluoperazine (TFP) is an antagonist observed to bind to calcium-saturated calmodulin ($(Ca^{2+})_4$-CaM) at ratios of 1:1 (1CTR), 2:1 (1A29), and 4:1 (1LIN). Each structure contains one TFP bound in the hydrophobic cleft of the C-domain of CaM. However, the orientation of the trifluoromethyl (CF_3) moiety differs among them: it is buried in the C-domain cleft of 1A29 and 1LIN, but protrudes from 1CTR. We report a 2.0 Å resolution crystallographic structure (4RJD) of TFP bound to the (Ca^{2+})-saturated C-domain of CaM (CaM_C). The asymmetric unit contains two molecules of $(Ca^{2+})_2$-CaM_C. Chain backbones were nearly identical, but the orientation of TFP in the cleft of chain A matched 1A29/1LIN, while TFP bound to chain B matched 1CTR. This was accommodated by a flip of the M144 sidechain and small changes in sidechains of M109 and M145. Docking simulations suggested that the rotamer conformation of M144 determined the orientation of TFP within the cleft of $(Ca^{2+})_2$-CaM_C. Chains A and B show that the open cleft of $(Ca^{2+})_2$-CaM_C is promiscuous in accepting TFP in reversed directions under the same crystallization conditions. Observing multiple orientations of an antagonist bound to a single protein highlights the challenge of designing highly specific pharmaceuticals, and may have importance for QSAR of other CF_3-containing drugs such as fluoxetine (anti-depressant) or efavirenz (reverse transcriptase inhibitor). This study emphasizes that a single structure of a complex represents an energetically accessible state, but does not necessarily show the full range of energetically equivalent states.

Keywords

molecular recognition; drug specificity; promiscuous binding; TFP; trifluoromethyl; CF_3; thermodynamics; energetics; alternate conformers; pharmaceuticals; QSAR

*To whom correspondence should be addressed. Telephone: (319) 335-7885. Fax: (319) 335-9570. madeline-shea@uiowa.edu.

Introduction

Calmodulin (CaM) is an essential eukaryotic protein critical to many calcium-mediated signal transduction pathways. It is small (148 a.a.), highly acidic (pI of 4) and comprised of two homologous 4-helix bundle domains (N and C) that are connected by a flexible linker.[1,2] Each domain binds two calcium ions cooperatively in paired EF-Hand motifs[3], and there are anti-cooperative interactions between domains.[4–6] Fluctuations in calcium levels are linked to many intracellular events by effects on CaM. When saturated with calcium ions, each domain of CaM adopts an "open" tertiary conformation that exposes a hydrophobic cleft that binds protein targets (e.g., CaM kinase II (CaMKII), or myosin light chain kinase (MLCK)),[7–10] resulting in calcium-dependent regulation of their activity.[11] The calcium-binding affinity of domains of CaM may be enhanced or diminished by binding to protein targets,[12,13] allowing CaM to regulate temporally and spatially distinct cellular processes at different calcium concentrations.

In addition to interacting with naturally occurring protein targets, $(Ca^{2+})_4$–CaM also binds drugs such as trifluoperazine (TFP) (Fig. 1A). TFP is a first-generation antipsychotic drug in the phenothiazine class that is primarily used in the treatment of schizophrenia and related mental disorders.[14,15] *In vitro* studies have shown TFP to be a CaM antagonist that acts by disrupting the association of CaM with its protein targets.[16,17] Prior studies have focused on the stoichiometry of TFP binding, as well as its effect upon the calcium-binding affinity of CaM.[18,19] We have previously shown that the stoichiometry of TFP binding to CaM is linked to its calcium-ligation state: two TFP bind to apo CaM while four bind to $(Ca^{2+})_4$-CaM.[19]

When associated with intracellular protein targets such as metabolic enzymes, cyclases, kinases, phosphatases, and receptors, the canonical conformation of $(Ca^{2+})_4$-CaM is compact and ellipsoidal.[20–22] A similar conformation has been observed in three structures of $(Ca^{2+})_4$-CaM-TFP complexes that were determined by crystallography. In these, 1 (1CTR[23]), 2 (1A29[24]) or 4 (1LIN[25]) molecules of TFP are bound to $(Ca^{2+})_4$-CaM; they each have a TFP-binding site in the cleft of the C-domain, but only one structure (1LIN[25]) has a TFP-binding site in the N-domain. Our earlier comparison of the chemical exchange behavior of the N- and C-domain of $(Ca^{2+})_4$-CaM upon binding TFP indicated that TFP binds with a higher affinity to the C-domain of $(Ca^{2+})_4$-CaM than it does to the N-domain.[19] This is consistent with the structure 1CTR having TFP bound only to the C-domain of CaM.

Superposition of the α-carbon atoms of these three TFP/$(Ca^{2+})_4$-CaM complexes had an RMSD of only 0.7 Å (Fig. 1A), indicating that their backbone conformations are identical. However, examination of the apparently shared TFP-binding site in all three structures shows that the orientation of the trifluoromethyl (CF_3) group of TFP in this site differs (Fig. 1B). In two cases (1A29 and 1LIN), it is buried in the hydrophobic pocket of the C-domain, while in the other (1CTR), it does not contact the pocket, but rather protrudes from it.

To gain further insight into the solutes or crystallographic factors that might determine orientation and stoichiometry of TFP in the hydrophobic cleft of the C-domain of CaM, we undertook structural studies of TFP bound to a calcium-saturated C-domain fragment of

mammalian CaM (residues 76–148 of $(Ca^{2+})_4$-CaM, hereafter referred to as $(Ca^{2+})_2$-CaM_C). Surprisingly, two opposite orientations of TFP were observed simultaneously in a single asymmetric unit containing two $(Ca^{2+})_2$-CaM_C chains.

Results and Discussion

Structures of TFP-$(Ca^{2+})_2$-CaM_C

The asymmetric unit of 4RJD contains 2 $(Ca^{2+})_2$-CaM_C molecules (chains A and B) with a total of 4 TFP molecules: one in the hydrophobic cleft of each CaM_C chain, and two bridging them. In Fig. 1C, for illustration, the TFP molecules are numbered from left to right. Only two TFP molecules (1 and 4) associate closely with the hydrophobic pocket of chains A and B of $(Ca^{2+})_2$-CaM_C (Fig. 1D, Supp. Fig. 1). This array is similar to that observed in the 4:1 TFP/$(Ca^{2+})_4$-CaM structure (1LIN[25]). However, the independent C-domain chains in 4RJD are rotated 180° relative to each other, compared to the N- and C-domains of CaM in 1LIN.

Comparison of TFP bound to chains A and B of $(Ca^{2+})_2$-CaM_C

The 2Fo-Fc electron density map[26] at 1σ contour level in 4RJD before the ligands were modelled in as shown in Fig. 1D clearly indicates that the CF_3 group of TFP molecules 1 and 4 occupy orientations that are reversed relative to each other. In Fig. 2A, a surface representation illustrates how the CF_3 group is inserted into the hydrophobic pocket (Fig. 2A) or protrudes out (Fig. 2B) of CaM_C. The orientation of the CF_3 group of TFP in chain A is similar to that in the 1:1 structure of TFP bound C-domain of $(Ca^{2+})_4$-CaM (1CTR.pdb[23]), whereas the orientation of the CF_3 group of TFP in chain B is similar to that in the 4:1 structure of TFP bound to the C-domain of $(Ca^{2+})_4$-CaM (1LIN.pdb[25]). Superpositions of the backbone α-carbon atoms of (i) chain A of $(Ca^{2+})_2$-CaM_C with 1CTR.pdb and (ii) chain B of $(Ca^{2+})_2$-CaM_C with 1LIN.pdb indicated that they each had an RMSD < 0.6 Å (Fig. 2B).

These differences are identical to those observed when superimposing the backbone α-carbon atoms of all three previous structures of $(Ca^{2+})_4$-CaM-TFP (RMSD = 0.7 Å; Fig. 1A), and are similar to that observed when superimposing the backbone α-carbon atoms of chains A and B of $(Ca^{2+})_2$-CaM_C bound to TFP (RMSD = 0.43 Å; Fig. 1C). These results seen in a single structure provide evidence that the differences in the orientation of the CF_3 group of TFP bound to the cleft of CaM_C observed in previous structures are more likely due to the intrinsic flexibility of some key residues in the binding pocket of CaM, than differences in experimental conditions or improperly assigned electron density as had been suggested.[23,24,27] Rather, each of the three previously determined structures of TFP/$(Ca^{2+})_4$-CaM captured one of the multiple orientations that TFP may occupy within the malleable hydrophobic pocket of the C-domain.

Methionines Surrounding TFP

To explore the molecular determinants governing the orientation of TFP in the hydrophobic pocket of CaM_C, sidechain conformations were compared after alignment of backbones (Fig. 2C). Positions of sidechaines of some surface residues varied, but most sidechains

within 4 Å of the common TFP-binding sites were identical. The comparison of sidechain orientations is highlighted in Fig. 2D in an all-atom morph between chains A and B generated by the Yale Morph Server[28] and visualized with PyMOL.[29] In Fig. 2E, an electrostatic potential surface of chain A calculated by PyMol highlights the hydrophobic cleft (white) and acidic exterior (red) of CaM which has an isoelectric point close to 4.

Within the TFP-binding site of each CaM_C, the most significant difference between chain A and B was the orientation of the sidechain of M144, which adopted differing rotamer conformations in response to the orientation of the CF_3 group of TFP (Fig. 2F). Two additional methionine residues, M109 and M145, also adopted alternative conformations, but with a much smaller difference between chains A and B.

Early studies of CaM-target interactions demonstrated the importance of methionine residues in the hydrophobic pockets of CaM for variability of target binding.[30] Features of methionine that contribute to its significance in allowing CaM to recognize many targets and drugs include (a) minimal enthalpic discrimination among the possible c3 torsion angles (providing energetic freedom to conform to variable target binding surfaces), and (b) the unusually large polarizability of its sulfur atom (providing a source for London dispersion forces that could make substantial contributions to the attraction of non-polar groups).[31]

Computational docking of TFP to $(Ca^{2+})_2$-CaM_C

Because protein crystallization favors observation of molecules in low energy conformations that form an ordered crystal lattice, the appearance of two orientations of TFP in 4RJD suggests that they have similar binding affinities for $(Ca^{2+})_2$-CaM_C. If one conformation had a significantly more favorable energy than the other, it would be expected to dominate the population. To explore the predicted free energies of binding, and whether the sidechain rotamer conformation of M144 is sufficient to select the experimentally observed orientations of the CF_3 group of TFP, the binding of TFP to chains A and B of 4RJD was simulated using *AutoDock Vina*.[32]

The results showed that *AutoDock Vina* correctly predicted the CF_3 group orientation of TFP in chain A for 90% of the 10 lowest energy models (i.e., those with the most favorable free energies), while a 70% success rate was seen for chain B. In Fig. 2G, the CF_3 group of these 10 best energy models are depicted as spheres and overlaid upon $(Ca^{2+})_2$-CaM_C. The free energies obtained for these models of TFP binding to chain A ranged from −7.2 to −6.9 kcal/mol, while a range of −7.8 to −7.2 kcal/mol was observed for TFP binding to chain B. These values were similar to our previously reported docking simulations of TFP binding to the C-domain of $(Ca^{2+})_4$-CaM.[19] These computations are consistent with the two observed conformations of TFP binding to the hydrophobic cleft of $(Ca^{2+})_2$-CaM_C being energetically similar, but not identical. To definitively resolve this conclusion, it would be critical to determine relative binding affinity with solution-based titration method that could distinguish these alternate conformations.

Methionine-Based Selectivity

There are four Met residues in the hydrophobic pocket of $(Ca^{2+})_2$-CaM_C. Degrado and colleagues dubbed these “methionine puddles”.[30] NMR studies by the Wand laboratory showed that the sidechain dynamics of residues in the hydrophobic pockets of $(Ca^{2+})_4$-CaM change from having unusually high mobility in free CaM to having dramatic perturbations in flexibility when bound to a peptide derived from a target (e.g. smMLCK).[33] Residue M124 becomes unpredictably more rigid than in free CaM, while the mobility of others (M109, M144 and M145) remained relatively high and unchanged.[33] Other studies of sidechain methyl dynamics indicated that M144 is highly dynamic with respect to the other Met residues in CaM.[34,35]

The general importance of M144 in CaM recognition of target proteins was highlighted in a comparative studies of compact CaM-drug or CaM-peptide complexes that revealed a tetrad of residues (F92, L105, M124, M144) in CaM_C termed the FLMM motif that consistently contacted the ligand in all complexes examined.[36,37] Of these four residues, the sidechain of M144 was the most variable in the conformation it adopted when interacting with the hydrophobic anchor residue of the ligand. Functional studies of CaM have also highlighted the importance of M144, showing that it was selectively photolabeled upon addition of two putative CaM-binding domain peptides, Bpa-3 and smMLCK-Bpa,[38] and oxidation of M144 was shown to block activation of plasma membrane Ca-ATPase.[39] Together, these studies demonstrate the significance of M144 in target binding and highlight the dynamic nature of this residue that allows for multiple modes of TFP binding to $(Ca^{2+})_2$-CaM_C.

TFP Binding to Other EF-Hand Proteins

Prior studies of TFP binding to the EF-hand domains of CaM had shown a single conformation of TFP bound to each domain. An example of differential binding of TFP to another EF-hand protein was observed in the crystallographic structure of a Ca^{2+}-S100A4-TFP complex (3KO0.pdb[40]). Like CaM, members of the S100 family of proteins consist of two EF-hand Ca^{2+}-binding motifs, and calcium binding to the C-terminal EF-hand causes a conformational change that exposes a hydrophobic cleft to which myosin-IIA binds. TFP binding to S100A4 inhibits its ability to depolymerize myosin-IIA filaments. TFP-binding induces the assembly of 5 TFP/Ca^{2+}-S100A4 dimers into a pentameric ring via interactions between 2 TFP molecules. As in the structure of the C-domain of CaM reported here, two independent copies of the pentamer were observed in the asymmetric unit and the orientation of the two TFP molecules in the S100A4 binding sites of each pentamer were different.[40] This serves as another example of the promiscuity of TFP binding to hydrophobic binding pockets in proteins and emphasizes the importance of obtaining equilibrium binding data, in conjunction with structures, to fully understand the antagonistic effect of TFP on protein function.

Closing Summary

In this 2.0 Å resolution study of TFP bound to $(Ca^{2+})_4$-CaM_C, there were 2 $(Ca^{2+})_4$-CaM_C and 4 TFP molecules observed per asymmetric unit (Fig. 1C). However, this does not appear to be a dimer; there was no protein-protein interface observed. Comparison of the hydrophobic pockets of chains A and B of $(Ca^{2+})_4$-CaM_C illustrated that the CF_3 group of

the TFP bound in the cleft of chain A was buried, but protruded from the cleft of chain B. This suggests that the differences in orientation of the TFP molecules observed in the previous crystallographic structures may not be attributable to differences in experimental conditions such as crystal growth or salts, but instead illustrate the gymnastic proclivities of methionine residues lining the clefts of $(Ca^{2+})_4$-CaM such that they can accommodate TFP in multiple orientations within “the” hydrophobic pocket. In fact, this pocket is more like a beanbag chair resting on a hard frame. This study emphasizes the need for future studies of dynamics and binding to provide deeper understanding of both the entropic and enthalpic components of the antagonistic effects of TFP on the functions of CaM.

The value of CF_3 in medicinal chemistry was recognized long ago as a tool for rigidifying compounds and helping them cross the blood-brain barrier[41] Given the pharmacological significance of fluorinated ligands in protein binding and interaction[42]; and the growing use of CF_3 moieties in drug discovery efforts[43], future studies examining the interaction of the drug Perazine (TFP-analog lacking CF_3) will help to uncover the role of the CF_3 group in CaM recognition of TFP.

Materials and Methods

Protein Overexpression

IPTG-induced over-expression of mammalian CaM_C (residues 76–148) was performed using transformed E. coli BL21(DE3) cells containing the recombinant pT7-7 vector expressing the C-domain of *Rattus norvegicus* CaM.[44] CaM_C was overexpressed in Luria-Bertani broth, and purified as previously described.[45] The recombinant CaM_C was 97–99% pure as judged by silver-stained SDS-PAGE gels and reversed phase HPLC. Protein concentration was determined by UV spectroscopy of CaM_C denatured with NaOH[46] or native at pH 7.4.[3]

Crystallization of TFP Bound $(Ca^{2+})_2$-CaM_C

Crystallization of TFP with $(Ca^{2+})_2$-CaM_C was performed by adding a 10-fold molar excess of TFP (Sigma-Aldrich, St. Louis, MO) to 500 nL of ~10 mg/ml $(Ca^{2+})_2$-CaM_C in 50 mM HEPES, 100 mM KCl, 1 mM $MgCl_2$, 5mM NTA, 50μM EGTA, pH 7.4, with 500 nL of 200 mM potassium thiocyanate, 20% polyethylene glycol 3350, pH 6.6 (solution PEG 62 Qiagen) as a hanging drop. The tray was incubated at 15° C for ~8 months, at which time a single rod-shaped crystal was observed. The crystal was cryo-protected with mother liquor containing 20% ethylene glycol prior to being flash-cooled at 100 K. Data were collected on this crystal at 100 K at the 4.2.2 synchrotron beamline at the Advanced Light Source at the Ernest Orlando Lawrence Berkeley National Laboratory, with a 150 mm crystal-to-detector distance. The program d*TREK was used to reduce and scale the data.[47]

The monoclinic crystal diffracted to a resolution of 2.0 Å and was of the space group P21. Molecular replacement was performed using the extracted C-domain of TFP bound $(Ca^{2+})_4$-CaM (1LIN.pdb) with the program Phaser.[48] TFP and calcium ions were removed from the coordinate template prior to use in molecular replacement. Refinement was performed using the program Refmac5 of the CCP4 program suite[49] and Phenix.[50] Coot[51] was used for

molecular visualization and model building. Calcium ions and TFP were modeled into clearly visible electron density: water molecules were finally added to the structure using Coot, followed by cycles of manual editing and refinement. Data collection and refinement statistics are reported in Table 1. Structure validation was performed with the RCSB PDB Data Validation and Deposition Services [52,53] and Molprobity[54,55]

Computational Modeling of TFP Binding

AutoDock Vina 1.0.3[32] was used to simulate the binding of a single molecule of TFP to either chain A or B after all TFP had been removed. A cubic (18 $Å^3$) search space with implicit water was centered within the hydrophobic cavity of each chain for docking of TFP. The exhaustiveness parameter was 128.

Coordinates

Atomic coordinates and structure factors of the TFP: $(Ca^{2+})_2$-CaM_C complex were deposited at the Protein Data Bank with accession number 4RJD.

Supplementary Material

Refer to Web version on PubMed Central for supplementary material.

Acknowledgments

Supported by the National Institutes of Health RO1 GM 57001 to M.A.S., and by the Roy J. Carver Charitable Trust Grant 01-224. We acknowledge use of the University of Iowa Carver College of Medicine Protein Crystallography Facility; S. Ramaswamy and Brenda R. Sorensen for helpful discussions, as well as Jay Nix at Ernest Orlando Lawrence Berkeley National Laboratory for assistance in data collection.

Abbreviations

CaM	Calmodulin
CaMKII	Calmodulin-Dependent Kinase II
smMLCK	smooth muscle Myosin Light Chain Kinase
TFP	Trifluoperazine

References

1. Babu, YS.; Bugg, CE.; Cook, WJ. Three-dimensional structure of calmodulin. In: Cohen, P.; Klee, CB., editors. Calmodulin. 256. Elsevier; 1988. p. 83-89.
2. Barbato G, Ikura M, Kay LE, Pastor RW, Bax A. Backbone dynamics of calmodulin studied by ^{15}N relaxation using inverse detected two-dimensional NMR spectroscopy: The central helix is flexible. Biochemistry. 1992; 31:5269–5278. [PubMed: 1606151]
3. Crouch TH, Klee CB. Positive Cooperative Binding of Calcium to Bovine Brain Calmodulin. Biochemistry. 1980; 19:3692–3698. [PubMed: 7407067]
4. Shea MA, Verhoeven AS, Pedigo S. Calcium-Induced Interactions of Calmodulin Domains Revealed by Quantitative Thrombin Footprinting of Arg37 and Arg106. Biochemistry. 1996; 35:2943–2957. [PubMed: 8608132]

5. Pedigo S, Shea MA. Quantitative endoproteinase GluC footprinting of cooperative Ca^{2+} binding to calmodulin: Proteolytic susceptibility of E31 and E87 indicates interdomain interactions. Biochemistry. 1995; 34:1179–1196. [PubMed: 7827068]
6. Sun H, Yin D, Coffeen LA, Shea MA, Squier TC. Mutation of Tyr138 Disrupts the Structural Coupling between the Opposing Domains in Vertebrate Calmodulin. Biochemistry. 2001; 40(32): 9605–9617. [PubMed: 11583160]
7. Klee, CB. Calmodulin: Structure-Function Relationships. In: Cheung, WY., editor. Calcium and Cell Function volI Calmodulin. New York: Academic Press; 1980. p. 59-77.
8. Bayley PM, Findlay WA, Martin SR. Target recognition by calmodulin: Dissecting the kinetics and affinity of interaction using short peptide sequences. Protein Sci. 1996; 5:1215–1228. [PubMed: 8819155]
9. Colbran RJ. Regulation and role of brain calcium/calmodulin-dependent protein kinase II. NeurochemInt. 1992; 21:469–497.
10. Persechini A, Kretsinger RH. Toward a Model of the Calmodulin-Myosin Light Chain Kinase Complex: Implications for Calmodulin Function. J Cardiovasc Pharmacol. 1988
11. O'Neil KT, Erickson-Viitanen S, Wolfe HR Jr, DeGrado WF. The Structural Basis for the Calmodulin-Amphiphilic Peptide Interaction. Biophys J. 1987; 51:451a.
12. Peersen OB, Madsen TS, Falke JJ. Intermolecular tuning of calmodulin by target peptides and proteins: differential effects on Ca^{2+} binding and implications for kinase activation. Protein Science. 1997; 6(4):794–807. [PubMed: 9098889]
13. Evans TIA, Shea MA. Domain-Specific Calmodulin Interactions with CaMKII. Biophysical Journal. 2006; 90:519a.
14. Abuzzahab FS. The treatment of schizophrenia with long-acting oral neuroleptics: a six-month double-blind investigation of penfluridol versus trifluoperazine. Psychopharmacol Bull. 1977; 13(3):26–27. [PubMed: 329326]
15. Oybir F. Trifluoperazine in chronic, withdrawn schizophrenics. Dis Nerv Syst. 1962; 23:348–350. [PubMed: 14482952]
16. Lydan, O'Day. Different Developmental Functions for Calmodulin in Dictyostelium: Trifluoperazine and R24571 Both Inhibit Cell and Pronuclear Fucion but Enhance Gamete Formation. ExpCell Res. 1988; 178:51–63.
17. Pelech SL, Jetha F, Vance DE. Trifluoperazine and other anaesthetics inhibit rat liver CTP: phosphocholine cytidylyltransferase. FEBS letters. 1983; 158(1):89–92. [PubMed: 6134645]
18. Matsushima N, Hayashi N, Jinbo Y, Izumi Y. Ca^{2+}-bound calmodulin forms a compact globular structure on binding four trifluoperazine molecules in solution. Biochem J. 2000; 347(Pt 1):211–215. [PubMed: 10727421]
19. Feldkamp MD, O'Donnell SE, Yu L, Shea MA. Allosteric effects of the antipsychotic drug trifluoperazine on the energetics of calcium binding by calmodulin. Proteins. 2010; 78(10):2265–2282. [PubMed: 20544963]
20. Meador WE, Means AR, Quiocho FA. Modulation of calmodulin plasticity in molecular recognition on the basis of X-ray structures. Science. 1993; 262:1718–1721. [PubMed: 8259515]
21. Hoeflich KP, Ikura M. Calmodulin in Action: Diversity in Target Recognition and Activation Mechanisms. Cell. 2002; 108:739–742. [PubMed: 11955428]
22. Mori M, Konno T, Ozawa T, Murata M, Imoto K, Nagayama K. Novel Interaction of the Voltage-Dependent Sodium Channel (VDSC) with Calmodulin: Does VDSC Acquire Calmodulin-Mediated Ca^{2+}-Sensitivity? Biochemistry. 2000; 39(6):1316–1323. [PubMed: 10684611]
23. Cook WJ, Walter LJ, Walter MR. Drug Binding by Calmodulin: Crystal Structure of a Calmodulin-Trifluoperazine Complex. Biochemistry. 1994; 33:15259–15265. [PubMed: 7803388]
24. Vertessy BG, Harmat V, Bocskei Z, Naray-Szabo G, Orosz F, Ovadi J. Simultaneous binding of drugs with different chemical structures to Ca^{2+}-calmodulin: crystallographic and spectroscopic studies. Biochemistry. 1998; 37(44):15300–15310. [PubMed: 9799490]
25. Vandonselaar M, Hickie RA, Quail JW, Delbaere LTJ. Trifluoperazine-induced conformational change in Ca^{+2}-calmodulin. Nature Structural Biology. 1994; 1(11):795–801.

26. Jones TA, Zou JY, Cowan SW, Kjeldgaard M. Improved methods for building protein models in electron density maps and the location of errors in these models. Acta crystallographica Section A, Foundations of crystallography. 1991; 47 (Pt 2):110–119.
27. Vandonselaar M, Hickie RA, Quail JW, Delbaere LT. Trifluoperazine-induced conformational change in Ca^{2+}-calmodulin. Nat Struct Biol. 1994; 1(11):795–801. [PubMed: 7634090]
28. Krebs WG, Gerstein M. The morph server: a standardized system for analyzing and visualizing macromolecular motions in a database framework. Nucleic Acids Res. 2000; 28(8):1665–1675. [PubMed: 10734184]
29. The PyMOL Molecular Graphics System. 1.5.0.4. Schrödinger, LLC;
30. O'Neil KT, DeGrado WF. How calmodulin binds its targets: sequence independent recognition of amphiphilic alpha-helices. Trends Biochem Sci. 1990; 15(2):59–64. [PubMed: 2186516]
31. Gellman SH. On the Role of Methionine Residues in the Sequence-Independent Recognition of Nonpolar Protein Surfaces. Biochemistry. 1991; 30(27):6633–6636. [PubMed: 2065050]
32. Trott O, Olson AJ. AutoDock Vina: Improving the speed and accuracy of docking with a new scoring function, efficient optimization, and multithreading. J Comput Chem. 31(2):455–461. [PubMed: 19499576]
33. Lee AL, Kinnear SA, Wand JA. Redistribution and loss of side chain entropy upon formation of a calmodulin–peptide complex. Nature Struct Biol. 2000; 7(1):72–77. [PubMed: 10625431]
34. Chen C, Feng Y, Short JH, Wand AJ. The main chain dynamics of a peptide bound to calmodulin. JBiolChem. 1993; 306:510–514.
35. Ehrhardt MR, Urbauer JL, Wand AJ. The energetics and dynamics of molecular recognition by calmodulin. Biochemistry. 1995; 34:2731–2738. [PubMed: 7893684]
36. Ataman ZA, Gakhar L, Sorensen BR, Hell JW, Shea MA. The NMDA Receptor NR1 C1 Region Bound to Calmodulin: Structural Insights into Functional Differences between Homologous Domains. Structure. 2007; 15(12):1603–1617. [PubMed: 18073110]
37. Ishida H, Vogel HJ. Protein-peptide interaction studies demonstrate the versatility of calmodulin target protein binding. Protein Pept Lett. 2006; 13(5):455–465. [PubMed: 16800798]
38. O'Neil KT, Erickson-Viitanen S, DeGrado WF. Photolabeling of Calmodulin with Basic Amphiphilic alpha-Helical Peptides Containing p-Benzoylphenylalanine. JBiolChem. 1989; 264(24):14571–14578.
39. Bartlett RK, Urbauer RJB, Anbanandam A, Smallwood HS, Urbauer JL, Squier TC. Oxidation of Met^{144} and Met^{145} in Calmodulin Blocks Calmodulin Dependent Activation of the Plasma Membrane Ca-ATPase. Biochemistry. 2003; 42:3231–3238. [PubMed: 12641454]
40. Malashkevich VN, Dulyaninova NG, Ramagopal UA, Liriano MA, Varney KM, Knight D, Brenowitz M, Weber DJ, Almo SC, Bresnick AR. Phenothiazines inhibit S100A4 function by inducing protein oligomerization. Proceedings of the National Academy of Sciences of the United States of America. 2010; 107(19):8605–8610. [PubMed: 20421509]
41. Yale HL. The trifluoromethyl group in medicinal chemistry. Journal of medicinal and pharmaceutical chemistry. 1959; 1(2):121–133. [PubMed: 13665284]
42. Bohm HJ, Banner D, Bendels S, Kansy M, Kuhn B, Muller K, Obst-Sander U, Stahl M. Fluorine in medicinal chemistry. Chembiochem : a European journal of chemical biology. 2004; 5(5):637–643. [PubMed: 15122635]
43. Barnes-Seeman D, Beck J, Springer C. Fluorinated compounds in medicinal chemistry: recent applications, synthetic advances and matched-pair analyses. Current topics in medicinal chemistry. 2014; 14(7):855–864. [PubMed: 24484427]
44. Sorensen BR, Shea MA. Interactions between domains of apo calmodulin alter calcium binding and stability. Biochemistry. 1998; 37:4244–4253. [PubMed: 9521747]
45. Putkey JA, Slaughter GR, Means AR. Bacterial expression and characterization of proteins derived from the chicken calmodulin cDNA and a calmodulin processed gene. Journal of Biological Chemistry. 1985; 260(8):4704–4712. [PubMed: 2985564]
46. Beaven GH, Holiday ER. Ultraviolet absorption spectra of proteins and amino acids. Advances in Protein Chemistry. 1952; 7:319–386. [PubMed: 14933256]
47. Pflugrath JW. The finer things in X-ray diffraction data collection. Acta Crystallographica Section D, Biological Crystallography. 1999; 55(10):1718–1725.

48. McCoy AJ, Grosse-Kunstleve RW, Adams PD, Winn MD, Storoni LC, Read RJ. Phaser crystallographic software. J Appl Crystallogr. 2007; 40(Pt 4):658–674. [PubMed: 19461840]

49. Murshudov GN, Vagin AA, Dodson EJ. Refinement of macromolecular structures by the maximum-likelihood method. Acta Crystallographica Section D, Biological Crystallography. 1997; 53(3):240–255.

50. Adams PD, Afonine PV, Bunkoczi G, Chen VB, Davis IW, Echols N, Headd JJ, Hung LW, Kapral GJ, Grosse-Kunstleve RW, McCoy AJ, Moriarty NW, Oeffner R, Read RJ, Richardson DC, Richardson JS, Terwilliger TC, Zwart PH. PHENIX: a comprehensive Python-based system for macromolecular structure solution. Acta crystallographica Section D, Biological crystallography. 2010; 66(Pt 2):213–221.

51. Emsley P, Cowtan K. Coot: model-building tools for molecular graphics. Acta crystallographica Section D, Biological crystallography. 2004; 60(Pt 12 Pt 1):2126–2132.

52. Berman H, Henrick K, Nakamura H. Announcing the worldwide Protein Data Bank. Nat Struct Biol. 2003; 10(12):980. [PubMed: 14634627]

53. Berman HM, Westbrook J, Feng Z, Gilliland G, Bhat TN, Weissig H, Shindyalov IN, Bourne PE. The Protein Data Bank. Nucleic Acids Res. 2000; 28(1):235–242. [PubMed: 10592235]

54. Davis IW, Leaver-Fay A, Chen VB, Block JN, Kapral GJ, Wang X, Murray LW, Arendall WB 3rd, Snoeyink J, Richardson JS, Richardson DC. MolProbity: all-atom contacts and structure validation for proteins and nucleic acids. Nucleic Acids Res. 2007; 35(Web Server issue):W375–383. [PubMed: 17452350]

55. Chen VB, Arendall WB 3rd, Headd JJ, Keedy DA, Immormino RM, Kapral GJ, Murray LW, Richardson JS, Richardson DC. MolProbity: all-atom structure validation for macromolecular crystallography. Acta Crystallogr D Biol Crystallogr. 2010; 66(Pt 1):12–21. [PubMed: 20057044]

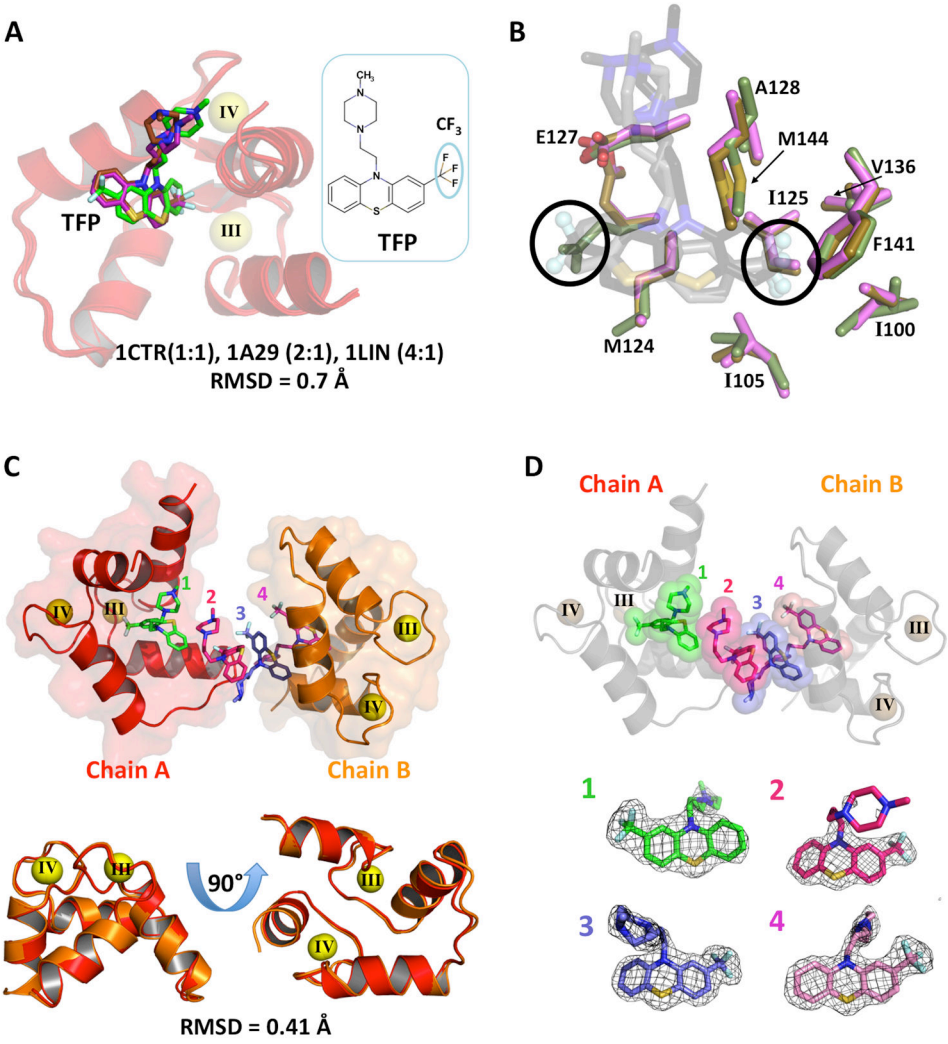

Figure 1.

A: Structures of TFP bound at a common C-domain site of $(Ca^{2+})_4$-$CaM_{1–148}$ and chemical structure of TFP. Superimposed structures of the α-carbon backbone atoms of TFP bound to the C-domain (red) of $(Ca^{2+})_4$-$CaM_{1–148}$ (N-domain not shown), with calcium ions (yellow spheres), and TFP (sticks) colored green, purple and brown corresponding to structures of TFP bound to $(Ca^{2+})_4$-$CaM_{1–148}$ at ratios of 1:1 (1CTR.pdb[23]), 2:1 (1A29.pdb[24]), and 4:1 (1LIN.pdb[25]), respectively. Inset box shows the chemical structure of TFP highlighting the position of the CF_3 moiety.

B: $(Ca^{2+})_4$-CaM residues involved in TFP binding at a common site in $(Ca^{2+})_4$-$CaM_{1–148}$. Position of sidechain atoms of $(Ca^{2+})_4$-CaM residues within 4Å of the common TFP binding site in TFP/$(Ca^{2+})_4$-$CaM_{1–148}$ complexes superimposed on the basis of their α-carbon backbone atoms are shown in light green (1:1), light purple (2:1), and light brown (4:1) sticks. TFP is shown in transparent sticks where the position of the CF_3 group in the 1:1, 2:1, and 4:1 structures has been highlighted to depict the 180° flip in TFP orientation.

C: Structure of TFP bound $(Ca^{2+})_2$-CaM_C. On top, chain A (red) and chain B (orange) are shown as ribbons inside of their transparent molecular surfaces; calcium ions (yellow

spheres), and TFP (sticks) are highlighted. On bottom, the α-carbon backbone atoms of chains A and B are superimposed to illustrate the similarity in their backbone conformations.

D: Location and 2Fo-Fc electron density map of TFP molecules bound to $(Ca^{2+})_2$-CaM_C at 1σ contour level. On top, $(Ca^{2+})_2$-CaM_C is shown in light gray ribbons, calcium ions are shown as light yellow spheres, and TFP (green, magenta, light blue, and pink) arrayed between chain A and B are shown as sticks inside of spheres displaying the van der Waals radii of each TFP atom. Shown below are TFP molecules 1 through 4 fit into their corresponding 1σ 2Fo-Fc electron density maps.

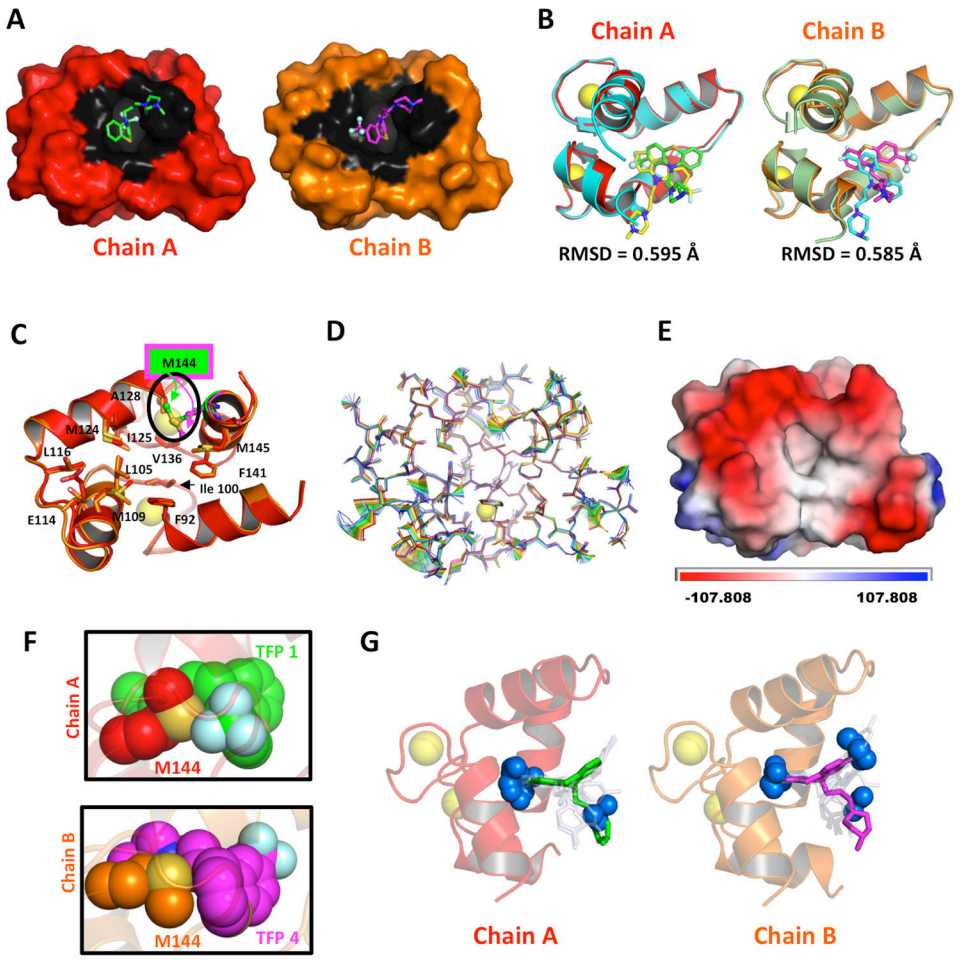

Figure 2.

A: Surface representation of $(Ca^{2+})_2$-CaM_C with bound TFP. Area representing residues within 4Å of either TFP-3 (green) bound to chain A (red) or TFP-1 (magenta) bound to chain B (orange) are colored black. The fluorine atoms of the CF_3 groups of TFP are shown as spheres to highlight the 180° rotation of TFP bound to chain A vs. chain B.

B: Comparison of TFP bound within the hydrophobic pocket of $(Ca^{2+})_2$-CaM_C and $(Ca^{2+})_4$-CaM. On left, α-carbon backbone atoms of chain A (red) were superimposed with the C-domain of the 1:1 TFP/$(Ca^{2+})_4$-CaM complex in 1CTR (cyan). On right, α-carbon backbone atoms of chain B (orange) were superimposed with the C-domain of the 4:1 TFP/$(Ca^{2+})_4$-CaM complex in 1LIN (light green). TFP are shown as green (chain A), magenta (chain B), yellow (1:1), and cyan (4:1) sticks. Calcium ions are represented as yellow spheres.

C: Comparison of $(Ca^{2+})_2$-$CaM_{76–148}$ TFP binding sites in clefts of chain A and B. The α-carbon backbone atoms of chain A (red) were superimposed with those of chain B (orange). Sidechain atoms within 4Å of the corresponding TFP binding site are shown as sticks, with M144 colored green (chain A) and magenta (chain B). Calcium ions are represented as yellow spheres.

D: A morph between chain A (blue) and B (red) generated by the Yale Morph Server[28] and illustrated using PyMOL[29]. Calcium ions shown as yellow spheres having 60% VDW radius.

E: The local protein contacts potential of chain A was generated using PyMOL.

F: Comparison of sidechain rotamer conformations adopted by M144 in $(Ca^{2+})_2$-CaM_C chain A (top) and B (bottom) in relation to TFP 1 (green) and TFP 4 (magenta); van der Waals radii of each atom are represented as spheres.

G: Docking simulations of TFP binding to $(Ca^{2+})_2$-$CaM_{76–148}$ using *Autodock Vina* 32. Chains A (red) and B (orange) of $(Ca^{2+})_2$-CaM_C are shown as ribbons. The experimentally observed positions of TFP in each chain are shown in green (chain A) and magenta (chain B). The 10 lowest energy positions of TFP are shown in transparent sticks; fluorine atoms of the CF_3 group are blue spheres.

Table 1

Data Collection and Refinement Statistics

Data collection	
Space group	P 1 21 1
Unit cell dimensions (Å)	a = 24.61, b = 85.64, c = 35.34
α, β, γ (°)	90.0, 93.0, 90.0
Number of molecules in the unit cell	4
Resolution range (Å)	27.23 – 2.0 (2.28-2.0)
Total number of measured reflections	9903
Number of unique reflections	8955 (1367)
Number of reflections for Rfree	426
Completeness of data (%)	(90.5/94.9)
*R_{sym} (%)	2.9 (11.8)
I/σ(I)	24.0 (8.1)
Redundancy	3.0 (3.0)
Refinement	
*R_{cryst} (%)	18.1
R_{free} (%) (5% data)	25.3
Number of atoms	1292
Protein atoms	1040
Ca^{2+}	4
TFP	112
H_2O	80
SCN	3
1PE	16
OXL	6
Cl	2
RMSD deviation from ideal geometry	0.010
RMSD in bond lengths (Å)	
RMSD in bond angles (°)	1.452
RMSD in dihedral angles (°)	20.088
Planarity (°)	0.004
Chirality (°)	0.049
Ramachandran plot (% residues)	98.44
Most Favored	1.56
Allowed	0
Disallowed	
Average B–factor ($Å^2$)	
Overall	31.9
Main chain atoms	27.1
Side chains and water molecules	35.3
Wilson Plot	21.0

Ca^{2+}	20.3
TFP	45.7
HOH	31.4
1PE	50.5
SCN	31.7
OXL	33.7
Cl	40.1
PDB Code	4RJD

Values in parentheses correspond to the values in the highest resolution shell.